

# The multi-stream flows and the dynamics of the cosmic web

**Sergei F. Shandarin**

Department of Physics and Astronomy, University of Kansas,  
10082 Malott Hall, 1251 Wescoe Hall Dr, Lawrence, Kansas, 66045, USA

E-mail: [sergei@ku.edu](mailto:sergei@ku.edu)

**Abstract.** A new numerical technique to identify the cosmic web is proposed. It is based on locating multi-stream flows, *i.e.* the places where the velocity field is multi-valued. The method is local in Eulerian space, simple and computationally efficient. This technique uses the velocities of particles and thus takes into account the dynamical information. This is in contrast with the majority of standard methods that use the coordinates of particles only. Two quantities are computed in every mesh cell: the mean and variance of the velocity field. In the cells where the velocity is single-valued the variance must be equal to zero exactly, therefore the cells with non-zero variance are identified as multi-stream flows. The technique has been tested in a N-body simulation of the  $\Lambda$ CDM model. The preliminary analysis has shown that numerical noise does not pose a significant problem. The web identified by the new method has been compared with the web identified by the standard technique using only the particle coordinates. The comparison has shown overall similarity of two webs as expected, however they by no means are identical. For example, the isocontours of the corresponding fields have significantly different shapes and some density peaks of similar heights exhibit significant differences in the velocity variance and vice versa. This suggests that the density and velocity variance have a significant degree of independence. The shape of the two-dimensional pdf of density and velocity variance confirms this proposition. Thus, we conclude that the dynamical information probed by this technique introduces an additional dimension into analysis of the web.

**Keywords:** cosmic web, cosmological simulations, cosmic flows

---

## Contents

<b>1</b>	<b>Introduction</b>	<b>1</b>
<b>2</b>	<b>The idea of the method</b>	<b>5</b>
<b>3</b>	<b>The numerical technique and N-body simulation</b>	<b>6</b>
3.1	Numerical technique	6
3.2	The cosmological model and simulation parameters	7
<b>4</b>	<b>The analysis of numerical noise</b>	<b>7</b>
4.1	Initial linear state	7
4.2	Final nonlinear state	8
<b>5</b>	<b>The total volume in voids</b>	<b>9</b>
<b>6</b>	<b>The multi-stream flows versus the density web</b>	<b>10</b>
6.1	The slice through a void	12
6.2	The slice through clumps and filaments	13
<b>7</b>	<b>The mean velocity field</b>	<b>14</b>
<b>8</b>	<b>Summary</b>	<b>14</b>

---

## 1 Introduction

The morphology of the cosmic web is an active field of research in modern cosmology. A wide variety of methods have been suggested, see *e.g.* [1, 2, 6, 7, 14, 17, 24, 26, 28] just to mention a few. However, all these methods share one common feature: they study the cosmic web as a property of the density field derived either from the distribution of particles in space in cosmological N-body simulations or from galaxies in the redshift space. However, the web can be viewed as a giant multi-stream flow. We suggest a simple technique that is capable to identify multi-stream flows and test it in a cosmological simulation of the  $\Lambda$ CDM model.

We begin with a short overview of the origin and evolution of the concept of multi-stream flows in the context of the formation of the large-scale structure in the universe. The notion of three-stream flows was introduced by Zeldovich [32], in his paper on pancakes. He briefly discussed the formation of three-stream flows and illustrated the formation of a three-stream flow by the evolution of Eulerian coordinate as a function of Lagrangian coordinate with time. However, he himself used it mainly as a useful auxiliary theoretical tool helping to describe the nonlinear structures known at present as "Zeldovich's pancakes". Before 1980 he himself seemed not to think that the multi-stream flows as a physical phenomenon might have relevance to the formation of the structures in the universe. Similar views were common in the west as well. For instance, multi-stream flows were barely mentioned in Peebles' book published in 1980 and it was only in the context of critical remarks on the pancake model.

Doroshkevich et al. [12] explored the evolution of the multi-stream flows in the one-dimensional N-body simulation a little beyond the three-stream flow stage up to seven streams. This simulation has shown that the multi-stream flow region remains relatively thin

in the comoving coordinates in contrast with a simple extrapolation of the Zeldovich approximation (ZA) where it grows unlimitedly. The quantitative comparison of the thicknesses of the three-stream flow in ZA and in the one-dimensional numerical simulation was presented in the review [29]. The geometry of generic caustics in ZA in two dimensions was discussed in [3], the authors also provided a table of generic singularities occurring in the potential flows in three-dimensional space. A detailed study of the phase space in self-similar gravitational collapse in one, two and three dimensions was presented in [13]. A high resolution two-dimensional distribution of particles obtained in ZA that clearly showed the structure of multi-stream flows was demonstrated in [8], and in the high-resolution two-dimensional N-body simulations in [22].

The multi-stream flows were directly addressed in the model based on the adhesion approximation (AA) suggested in [15]. The AA model was designed to control the runaway growth of the thickness of the pancakes in ZA by introducing artificial viscosity term in the Euler equation. This term has no effect on the motion in voids leaving it as it was in ZA but does not allow the formation of multi-stream flows by annihilating the transverse to pancakes or filaments velocities. Thus, the high density walls and filaments are formed in AA instead of multi-stream flows in ZA. The density profile controlled by the adopted value of the viscosity coefficient becomes smooth and the velocity remains single valued. It is worth stressing that AA modifies the multi-stream flows by transforming them in single-stream flows of a special kind, characterized by high density. An important feature of the model consists in allowing the mass flow within the pancakes and filaments. The model incorporates most of the features of the hierarchical clustering process which is characteristic of the cosmological models dominated by cold dark matter. In addition, the AA model predicted several new features including the continuous flow of mass from walls to filaments to clumps, the multiple merger of clumps, the collapse of some voids, the presence of substructure of hierarchical type in voids, formation of the next generations of the filaments and pancakes. It was quantitatively tested against the two-dimensional [19] and three-dimensional [23] N-body simulations and was also used for predicting the structure in the forthcoming SDSS [30, 31].

Another significantly simpler modification of ZA was suggested in [9]. Since the ZA model has a serious problem with the runaway growth of the three-stream flow regions the authors proposed to filter out the perturbations with the scales smaller than the scale of nonlinearity *i.e.* the scale corresponding to the r.m.s density contrast fluctuation being equal to unity. The tests of the model dubbed the truncated Zeldovich approximation (TZA) against three-dimensional N-body simulations generally confirmed what was expected: the large-scale structure was reproduced quite accurately but the structures on small scales were erased. Two years earlier it had been shown that even replacing the small-scale perturbations with a new statistically independent realization would not change significantly the large-scale structure [20]. The large-scale structure proved to be quite robust. The evolution of the structure with time could be crudely probed by generating a sequence of particle distributions using TZA with the scale of nonlinearity corresponding to each chosen epoch.

A very similar modification of ZA as far as the large-scale dynamics is concerned was suggested by Bond, Kofman and Pogosyan [5] (the BKP model). The only but crucial difference between the BKP and TZA models consists in a different choice of the scale separating the large-scale and small-scale dynamics. The authors of BKP model strongly stressed that the boundary must be chosen in such a way that the large-scale motion was strictly single-stream flow. The authors also emphasized the coherence of the filtered linear density field and derived from it the strain tensor field on the scales of tens of Mpc between rare high

density peaks, the idea somewhat similar to the proposition made earlier in [10, 11] and [31]. The presence of this coherence causes the appearance of filaments and possibly pancakes. However, the chosen condition for the scale separating large-scale dynamics from small scale dynamics means that the filaments are the enhancements of density but not multi-stream flows. This is contrary to both the TZA and AA models.

It is probably worth mentioning one more difference between AA on the one hand and TZA and BKP on the other although it is of a rather technical kind. The TZA and BKP models similarly to ZA use the the strain tensor as a primary initial field (referred to as the deformation tensor in TZA). The AA model is based on the linear velocity potential defined by the relation  $\mathbf{v} = -\nabla\Phi_v$ , which coincides up to a constant factor with the linear gravitational potential in the growing mode. In principle, both the velocity potential and strain fields contain exactly same information since one of them can be easily computed from the other. However, repackaging of the same information may be useful if it helps to identify the most significant variable that determines the structure or serves a particular goal of the model better. Summarizing this short discussion of three theoretical models of the large-scale structure we stress one difference essential for this paper. The multi-stream flows are characteristic for both TZA and AA while the BKP model eludes them in the large-scale dynamics.

The ZA model defines pancakes as the regions between the surfaces on which the density is formally singular *i.e.* as the multi-stream flows. The three-dimensional N-body simulation by Klypin and Shandarin [18] revealed that the most conspicuous features after clumps are filaments rather than pancakes. Combining this finding with the results of [3] naturally caused the definition of filaments to become similar to that of pancakes: filaments are the multi-stream flows having very oblong shapes. The similarity is based on dynamics, the both pancakes and filaments are nonlinear but unvirialized concentrations of mass therefore in the dynamical hierarchy they hold an intermediate position between the density peaks that have not collapsed yet and virialized halos. At the same time another commonly used definition of objects as peaks above certain height in the density field [4] was also broadened to include pancakes and filaments [5]. On the one hand the former is more physical but at the time seemed to be harder to implement especially when the dynamical information about the structure was scarce. On the other the latter seems to be more practical but involves a free parameter, the threshold that determines which peak should be considered an object. This difference between two definitions was probably the reason of the strongest discrepancy between the models declared in [5]: the formation of the objects in BKS is in inverse order than in ZA. It is worth pointing out that despite considerable overlapping between two definitions the objects they describe are not identical.

Despite the inability of current N-body simulations to resolve properly the phase space there is no doubt that the multi-stream flows must be present in the collisionless medium in the nonlinear regime. Therefore even the limited information about multi-stream flows would introduce a new dimension into the analysis of the cosmic web as it does in virialized halos [21]. This must be based on using the velocity field. Velocities bring about dynamical information totally independent of the density and gravitational potential fields in a general case. There are of course special cases like the systems in virial or thermal equilibrium where certain relations of statistical nature between velocities, coordinates of the particles and gravitational potential could be derived.

Recently there have already been made some attempts to incorporate dynamical information into the analysis of cosmic web [14, 17]. Both approaches are based on the analysis

of the eigen values of the Hessian of the gravitational potential at the nonlinear stage. Both groups appeal to the analogy with ZA and claim that this statistics provides a dynamical classification of the cosmic web. The only difference between two approaches is in the different choices of the amplitude to be assigned to the eigen values of the Hessian. However, as we have already mentioned neither density nor gravitational potential contain dynamic information in a general case since the both are computed from the particle coordinates only and absolutely independent of the velocities. We have already mentioned a couple of special cases when the gravitational potential and velocities could be related in statistical sense. The growing mode in the linear regime represents another special case. The dynamical evolution in ZA is described by a map  $\mathbf{x}(\mathbf{q}, t) = \mathbf{q} - D(t)\nabla\Phi_v(\mathbf{q})$ , where  $\Phi_v$  is the velocity potential *not the gravitational potential*. It is only due to the degeneracy of the growing mode in the linear regime where the velocity potential proportional to the gravitational potential  $\Phi_v = \text{constant} \times \Phi_g$  they can be used interchangeably with the proper choice of the constant. Therefore the gradient of the gravitational potential is proportional to the velocity and it can be computed from the gravitational potential in the growing mode in the linear regime. The ZA model is of course an extrapolation and therefore required additional scrutiny before it was excepted as a reasonable approximation for the initial phase of the nonlinear regime (see *e.g.* [29]). However, neither the gradient of the potential can be used for mapping nor its second derivatives represent the deformation tensor in a general case. If correct the reasoning presented in [17] and [14] must be valid for arbitrary velocities of the particles since the analysis and thus the conclusions do not depend on the velocities at all. This hardly can be true. Thus, even the suggested statistics may provide some merits for the study of the density and gravitational potential fields at the nonlinear stages its interpretation as a dynamical characteristics cannot be excepted in the present form.

The goal of the paper is to introduce a new numerical technique to identify the cosmic web as the multi-stream flows and present the results of the first tests, which are very encouraging. The method is based on a simple statistics derived from the coordinates and velocities of the particles: the mean and variance of velocities in every mesh cell. Here we use a uniform spatial mesh although the homogeneity of the mesh is not required by the method. We estimate the role of noise caused by numerical effects and compute the two-dimensional pdf of the density and variance of velocity which demonstrates a significant level of independence of these quantities. We compare the appearance of the multi-stream flow web with the web derived from the density field only as well as with the distribution of the particles themselves.

Although there is no agreement between different groups on the exact definition of the filaments and walls/pancakes the most agree that the filaments comprise more mass than any of the rest constituents of the web (*i.e.* clusters/clumps, walls/pancakes, field/void). For instance, the fraction of mass in filaments and walls in the  $\Lambda$ CDM simulations to be almost 50% of the total mass, considerably more than in clusters [1]. Both filaments and walls are nonlinear but unvirialized objects in contrast to clusters/clumps which are mostly virialized objects. The suggested method allows to quantitatively analyze the dynamics of these objects because they are multi-stream flows. This work is under way and the results will be reported in detail in a separate paper.

The rest of the paper is organized as follows. Section 2 describes the idea of the method, Sec. 3 describes the numerical technique and N-body simulation used in the tests, the noise analysis is given in Sec. 4. The total volume devoid of multi-stream flows is evaluated in Sec. 5. The appearance of the multi-flow web is compared with the density based web in

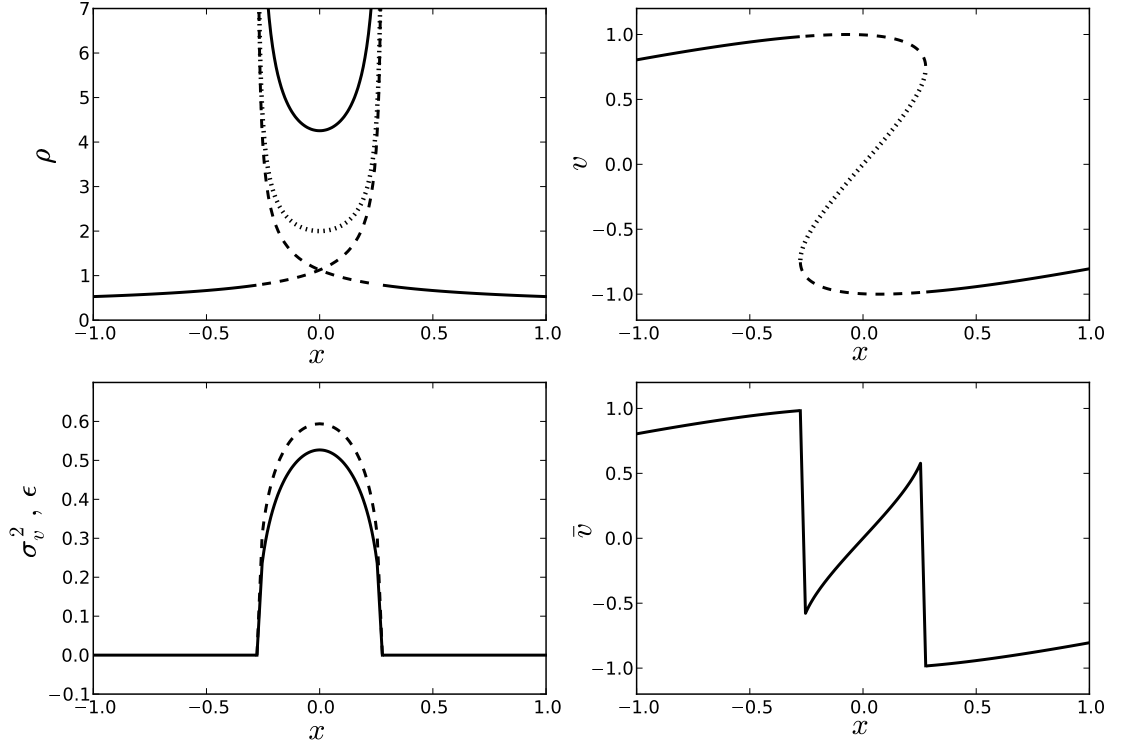


**Figure 1.** Top left panel. The density as a function of the Eulerian coordinate,  $x$ , is shown for all streams by dotted and dashed lines. The total density is shown by a solid line. Top right panel. The velocity in three streams are shown by dashed and dotted lines, the solid line shows the velocity outside the three-stream flow. Bottom left panel. The solid and dashed lines show respectively  $\sigma_v^2$  and  $\epsilon$  defined in eq. 2.2. Bottom right panel shows the mean velocity defined in eq. 2.3.

Sec. 6, and the mean velocity field is shown in Sec. 7. Finally the results are summarized in Sec. 8. In the rest of the paper density is given in the units of the mean dark matter density, velocities in km/s and  $\sigma_v^2$  in (km/s)<sup>2</sup>.

## 2 The idea of the method

The physical idea of the method can be illustrated by a simple example. Let us consider the formation of a one-dimensional pancake in ZA for a simple sinusoidal perturbation [3, 29, 32]. Using the comoving coordinates one can easily write down explicit expressions for the position, velocity and density as a function of the Lagrangian coordinate  $q$  and the linear growth factor  $D$  that can effectively play the role of time

$$x = q - D \sin q, \quad v \equiv dx/dD = -\sin q, \quad \rho = |1 - D \cos q|^{-1}. \quad (2.1)$$

The solution predicts a shell-crossing singularity in density at  $x = 0$  at  $D = 1$  and the formation of a three-stream flow afterward. At small  $\delta D = D - 1$  it approximately describes the generic phase space structure of the shell crossing regions at their early stages. At later

times it evolves into a multi-stream flow with five then seven etc. streams which is beyond the scope of ZA. The density and velocity profiles in the three-stream flow and its vicinity are shown in the top panels in Fig. 1. The velocity and density are shown for each stream in addition the total density in the three-stream flow region is also shown. Two bottom panels show the mean velocity, velocity variance  $\sigma^2$  (solid line) and the density of kinetic energy  $\epsilon$  (dashed line) defined below.

Usually the analysis of the structure of multi-stream flows is limited to the discussion of velocity and density fields. We propose to examine two additional quantities of thermodynamic and therefore statistical kind similar to density. One of them is the variance of velocity,  $\sigma_v^2(x)$ , and the other is the mean kinetic energy  $\epsilon(x)$  at every Eulerian point  $x$

$$\sigma_v^2(x) \equiv \frac{\sum_{i=1}^{n_s} \rho_i(x) \Delta v_i^2(x)}{\sum_{i=1}^{n_s} \rho_i(x)}, \quad \epsilon(x) \equiv \frac{\sum_{i=1}^{n_s} \rho_i^2(x) \Delta v_i^2(x)}{\sum_{i=1}^{n_s} \rho_i(x)}, \quad (2.2)$$

where  $\rho_i(x)$  and  $v_i(x)$  are the density and velocity in each stream and  $\Delta v_i \equiv v_i(x) - \bar{v}(x)$ ,  $n_s$  is the number of streams. The mean velocity is defined as

$$\bar{v}(x) \equiv \frac{\sum_{i=1}^{n_s} \rho_i(x) v_i(x)}{\sum_{i=1}^{n_s} \rho_i(x)}. \quad (2.3)$$

Figure 1 shows all these quantities at the nonlinear stage when the shell crossing has already happened and the three-stream flow has formed. Passing by we note that the mean velocity of the three-stream flow does not coincide with the velocity in one of the streams as may appear in the figure, but they are quite similar in this particular example.

Comparing the shapes of  $\sigma_v^2$  and  $\epsilon$  curves with the density and velocity curves we see remarkable differences. The most important, however not surprising feature of the  $\sigma_v^2$  and  $\epsilon$  curves is that they are identical zeros beyond the multi-stream flow regions. Less obvious and more surprising feature is that their shapes are so similar to each other and practically inverse to the shape of the total density curve in the shell crossing region. The both features suggest that the  $\sigma_v^2$  and  $\epsilon$  functions could be complimentary characteristics to the density in the studies of the dark matter cosmic web. The fact that they are equal exactly to zero beyond the multi-stream flow regions may mean that they can be good tracers of multi-stream flows. However, the discussed example is too oversimplified. In the reality the noise caused by discreteness undoubtedly violates this ideal situation and therefore must be taken into account before one can come to a sound conclusion. But first we describe the numerical technique.

### 3 The numerical technique and N-body simulation

#### 3.1 Numerical technique

Since  $\sigma_v^2$  and  $\epsilon$  are so similar we shall limit the discussion to  $\sigma_v^2$  only. The velocity variance depends on density less than  $\epsilon$  and therefore it carries more independent information. The physical dimensions of  $\sigma_v^2$  suggest that it can be directly related to the gravitational potential. However a more thorough analysis may reveal some additional attractive features of  $\epsilon$ .

We use the standard CIC (cloud-in-cell) method for the evaluation of  $\bar{v}$  and then  $\sigma_v^2$ . The particles are modeled as constant density cubes of size  $l = L/N_p$  where  $L = 512 \text{ h}^{-1}$  is the size of the simulation box and  $N_p = 512$  is the number of particles in one dimension. Both  $\bar{v}$  and  $\sigma_v^2$  are evaluated on a uniform cubic mesh with the cells of the same size as



that of particles. However, it is worth mentioning that the uniformity of the mesh is not a requirement of the method. In general each particle contributes a volume weighted fraction of its velocity to eight neighboring mesh sites. Each velocity fraction equals the fraction of the volume of the overlap of the particle cloud with the mesh cell. It also can be viewed as a fraction of its linear momentum since all the particles have the same masses. The mean velocity assigned to the mesh point is the sum of the contributions from all the particles overlapping with it divided by the total mass in the cell. The variance  $\sigma_v^2$  is evaluated in a similar manner. It is worth stressing that we conduct the further analysis without additional filtering of the density field which is also computed using the CIC scheme.

### 3.2 The cosmological model and simulation parameters

We applied this method to the pure dark matter N-body simulation in the  $512 h^{-1}\text{Mpc}$  cubic box using PM (particle mesh) code [16, 27]. The number of particles was  $512^3$  and the mesh in the gravitational force solver was  $1024^3$ . The parameters of the  $\Lambda\text{CDM}$  cosmological model were as follows:  $h = H_0/(100 \text{ km/s} \cdot \text{Mpc}) = 0.72$ ,  $\Omega_{\text{tot}} = 0.25$ ,  $\Omega_b = 0.043$ ,  $n = 0.97$ ,  $\sigma_8 = 0.8$ , the initial redshift  $z_{\text{in}} = 200$ . The choice of the parameters is related to the main purpose of the study: to test this new technique and illustrate its performance by applying it to a realistic cosmological model.

## 4 The analysis of numerical noise

We begin with applying this method to the initial state when all the fields are in the linear regime.

### 4.1 Initial linear state

Even at the very beginning the small displacements of particles from unperturbed positions on the regular grid result in small overlapping of particles with each other. It is also easy to imagine that more than one particle may overlap a mesh cell. This results in generating of small but nonetheless nonzero  $\sigma_v^2$ . The left hand side panel in Fig. 2 shows three functions  $f(v_p^2) = n(v_p^2)/512^3$  (in blue),  $f(\bar{v}^2)$  (in green) and  $f(\sigma_v^2)$  (in red), which are the fractions of particles or cells per equally sized logarithmic bins. In the ideal situation one expects that  $f(v_p^2) = f(\bar{v}^2)$  and  $f(\sigma_v^2) \equiv 0$  as it was described in Sec. 2. The first condition is satisfied with high accuracy and the second is obviously violated. However, the  $\sigma_v^2$  is approximately three orders of magnitude smaller than  $v_p^2$  or  $\bar{v}^2$  therefore we conclude that this test is passed without serious problem. In the multi-stream flows the  $\sigma_v^2$  is expected to be less than  $v_p^2$  but not orders of magnitude smaller (see Fig. 1 for an illustration).

An additional question may occur. Does the generation of noise in  $\sigma_v^2$  depend on the density in the cell? Naively one may think that  $\sigma_v^2$  is generated in the regions where particles are crowded and much less in the underdense regions with  $\rho < 1$  where the particles are deserted. The answer to this question happens to be not that simple as the left hand side panel in Fig. 3 shows. The figure displays the two-dimensional histogram  $f(\rho, \sigma_v^2)$  for the initial state. The maximum of the function is at  $\rho \approx 1$ ,  $\log_{10}(\sigma_v^2) \approx 5.5$ . The peak has approximately a triangle shape, extending to somewhat higher values of  $\sigma_v^2$  for both higher and lower densities. The third direction is downward to lower values of  $\log_{10}(\sigma_v^2)$ . This relatively complicated shape of  $f(\rho, \sigma_v^2)$  indicates that the kinematics of particles is not simply contraction for  $\rho > 1$  and expansion for  $\rho < 1$  even at this early stage. The overall shape of the histogram shows no strong correlation between  $\sigma_v^2$  and  $\rho$ .



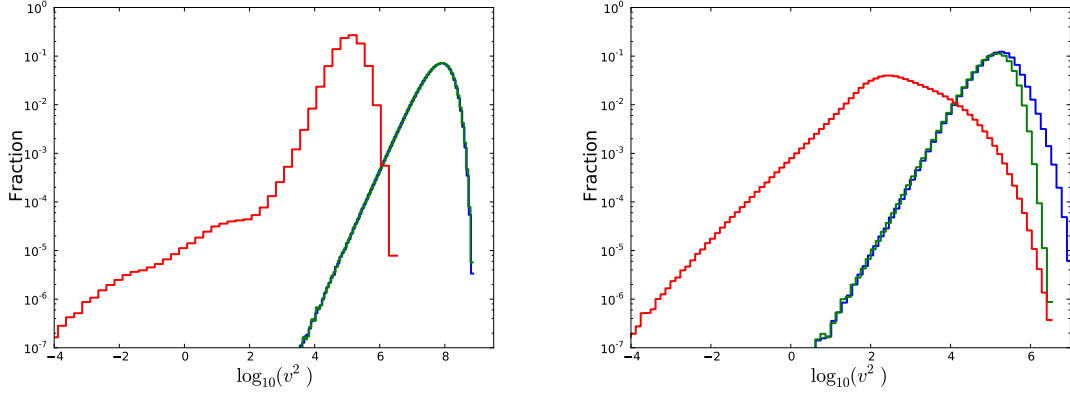


**Figure 2.** The fraction of particles per bin as a function of  $v_p^2$  (blue histograms), the fraction of mesh cells per bin as a function of  $\bar{v}^2$  (green histograms), and as a function of  $\sigma_v^2$  (red histograms) are shown for the initial state in the left hand side panel and for the present time in the right hand side panel. The fraction of particles with  $v_p^2$  and the fraction of cells with  $\bar{v}^2$  since  $v_p^2 = \bar{v}^2$  in the one-stream flow regions, thus the green and blue curves are one on top of the other in the left panel. There are also 33.4% of cells with  $\sigma_v^2 < 10^{-9}$  not shown in the right hand panel.

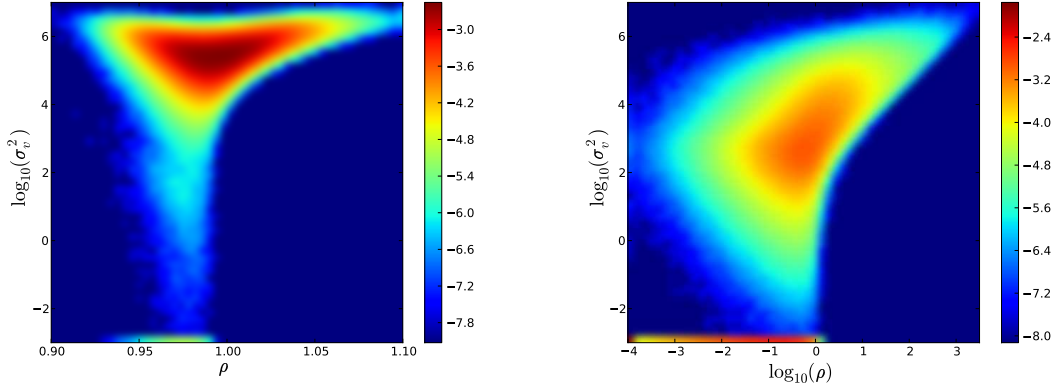


**Figure 3.** The fraction of cells  $n(\rho, \sigma_v^2)/512^3$  in bins as a function of  $\rho$  and  $\sigma_v^2$ . The color bars show the logarithmic scales for each panel. The both histograms are of same size  $50 \times 50$  with equally spaced bins along the axis marked in each panel. Left: the initial linear state. Right: the final highly nonlinear state.

## 4.2 Final nonlinear state

The statistics  $f(v_p^2)$ ,  $f(\bar{v}^2)$ ,  $f(\sigma_v^2)$ , and  $f(\rho, \sigma_v^2)$  look quite differently at the nonlinear stage. The right hand side panel in Fig. 2 shows the histograms for the first three functions. Only  $f(v_p^2)$  and  $f(\bar{v}^2)$  below the maximum are similar. At the high value end  $f(\bar{v}^2)$  drops considerably faster than  $f(v_p^2)$  since the mean velocity in the multi-stream flow regions is significantly lower than the velocities of particles (see also Fig. 1). The high value end of  $f(\sigma_v^2)$  is much closer to that of both  $f(v_p^2)$  and  $f(\bar{v}^2)$  as one may naturally expect for the multi-stream flow regions. It is worth mentioning that the highest mean velocities are greater than the highest relative velocities inside multi-stream flows.

As many as 11.76% of cells have  $\sigma_v^2 = 0$  exactly in excellent agreement with the fraction

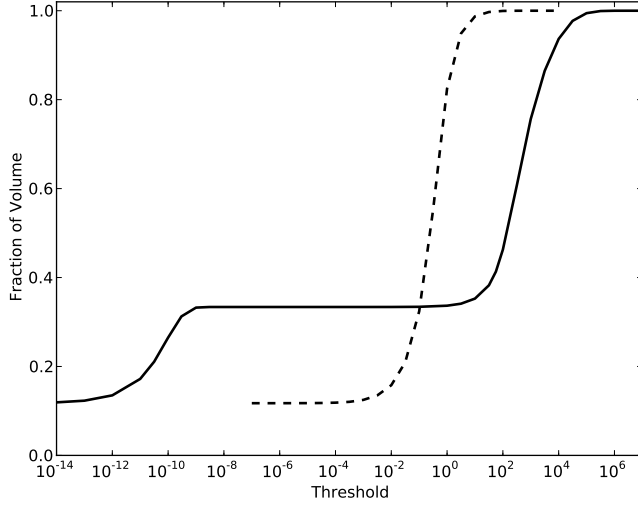


**Figure 4.** The fraction of volume where  $\sigma_v^2$  (solid line) or  $\rho/\bar{\rho}$  (dashed line) is less than the threshold. The horizontal gives the threshold in  $(\text{km/s})^2$  for  $\sigma_v^2$  and in dimensionless units for  $\rho/\bar{\rho}$ . The low limit for both quantities is the same 11.7% which is the fraction of sites where the density is zero exactly in the N-body simulation.

of completely empty cells with  $\rho = 0$  being equal to 11.74% , in addition there are 21.6% of cells with  $0 < \sigma_v^2 < 1 \times 10^{-9}$ . This explains the presence of red bar at the bottom of Fig. 3 (right panel). The two-dimensional histogram  $f(\rho, \sigma_v^2)$  shown in the right hand side panel of Fig. 3 is also substantially different from the linear case. There is an easily seen correlation between  $\sigma_v^2$  and  $\rho$ , at  $\rho > 1$ . However, the spread is about two orders of magnitude along the both directions for the red peak. The former is naturally related to the correlation of the gravitational potential depth with the high density peaks. The latter suggests that many medium density peaks ( $10 < \rho < (\text{a few}) \times 100$ ) as well as the filaments are not relaxed systems with  $\sigma_v^2$  in such cells to be almost independent of  $\rho$ .

## 5 The total volume in voids

There are 11.74% of the mesh cells completely empty, they obviously have  $\sigma_v^2 = 0$  exactly as well (except a tiny fraction due to numerical errors). However, additional 21.6% of cells have such a tiny  $\sigma_v^2 < 10^{-9}$  that they can be considered belonging to one-stream flow regions without doubts. The fractions of cells one as a function of density and the other as a function of  $\sigma_v^2$  where the corresponding quantity is less then the threshold shown in the horizontal is shown in Fig. 4. The function of  $\sigma_v^2$  grows from 33.24% at  $\sigma_v^2 = 1 \times 10^{-9}$  to 33.67% at  $\sigma_v^2 = 1$  and to 35.26% at  $\sigma_v^2 = 10$ . Then the rate of growth becomes significantly greater and the fraction  $f(\sigma_v^2)$  reaches 46.27% and 60.70% at  $\sigma_v^2 = 100$  and 316 respectively. The long plateau from  $\sigma_v^2 = 10^{-9}$  to about 10 (ten orders of magnitude!) shows that in about one third of the volume the velocity is a single valued function, *i.e.* no multi-stream flow regions are present there. This number can serve as a low physical limit for the total volume in voids for the resolution of this simulation. For a given mass resolution of N-body simulations one can give a physical definition of voids as the regions where the shell-crossing has not yet occurred. Therefore neither halos nor filaments nor sheets could have formed in these

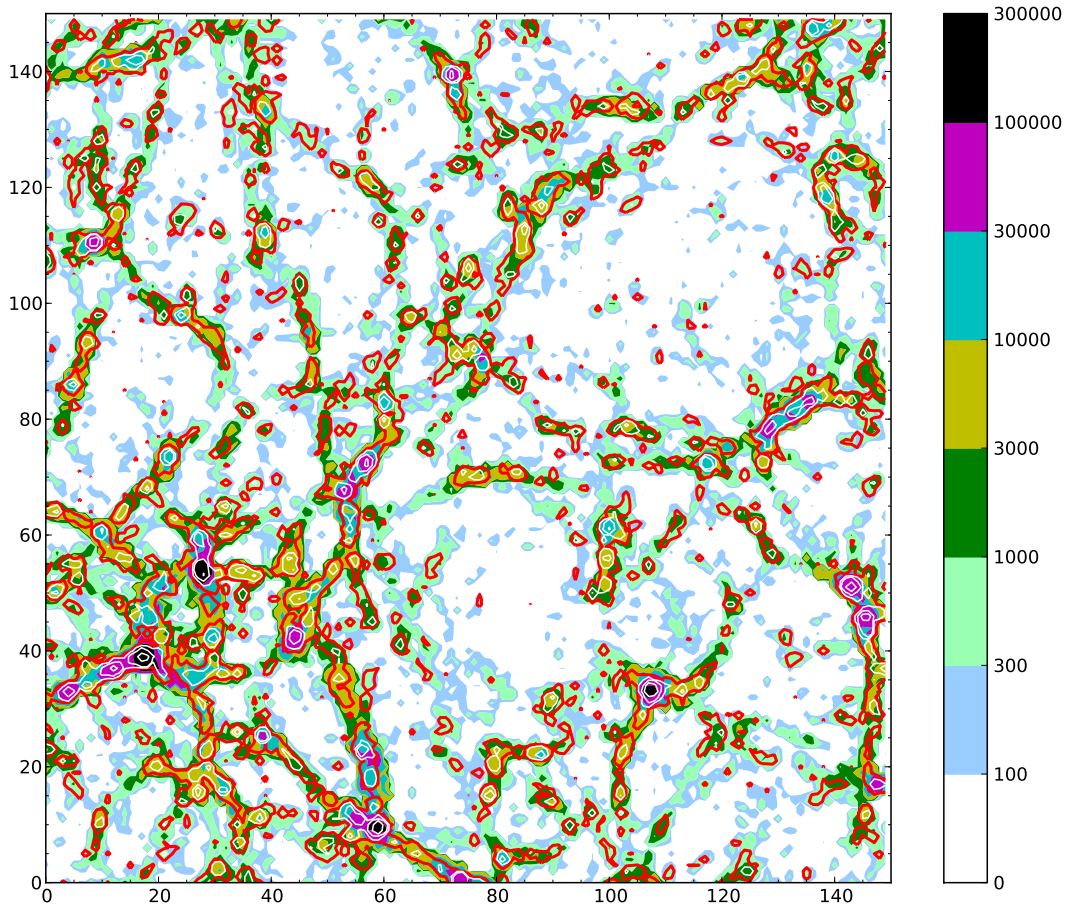


**Figure 5.** A part of a thin slice of  $1 h^{-1}$  Mpc thickness through N-body simulation box. The filled contours show the values of  $\sigma_v^2$  as indicated by the color column. Heavy red contours show the CIC density field with  $\rho = 1$ , the white thin contours inside red contours show  $\rho = 3, 10$  and  $50$ . The labels show the distances in  $h^{-1}$  Mpc.

regions. The multi-stream flow regions can apparently appear in such places with the growth of the resolution of the simulation.

## 6 The multi-stream flows versus the density web

In this section we compare the multi-flow web with the standard representation of the web by the isocontours of the dark matter density. Figure 5 shows the density contours superimposed on the field of  $\sigma_v^2$  in a thin slice ( $1 h^{-1}$  Mpc) randomly selected from the simulation cube. The filled contours show the regions of the  $\sigma_v^2$  field between the levels marked on the color column. The density contours correspond to the following levels: red to  $\rho = 1$  and three white contours correspond to  $\rho = 3, 10$  and  $50$ . One can see that although the overall structures are

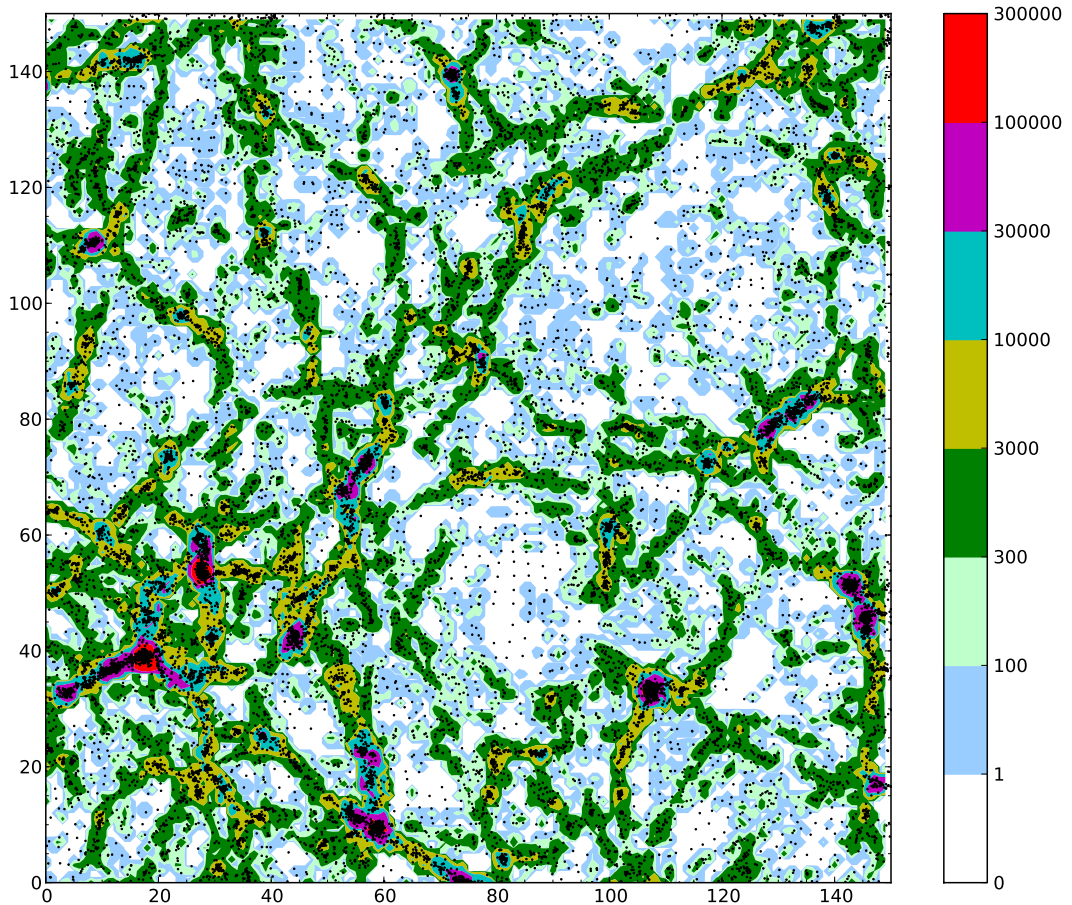


**Figure 6.** The same slice as in Fig. 5. The filled contours show the regions with  $\sigma_v^2$  displayed by the color column. Dots are the particles contributed to the density and  $\sigma_v^2$  in this slice.

very similar, but they by no means are identical. We consider the both observations as good news. The former is the evidence of the robustness of the identification of the filaments and other structures while the latter suggests that dynamical information in the  $\sigma_v^2$  field brings an additional dimension to the characteristics of the web. A closer inspection show that the highest peaks in two fields do not have identical shapes. It will be better seen in the following figures where we zoom up two regions: one with the lowest mean density (void region) and the other with the highest density in the slice (clumps and filaments).

However, we first show the superposition of particles contributing to the density and  $\sigma_v^2$  in this slice on the  $\sigma_v^2$  field in Fig. 6. The color map is slightly different from the previous figure, which allows to see the structures at low values of  $\sigma_v^2$  better. In general, we conclude that the correspondence of two fields it very good as it should be apart from numerical noise.

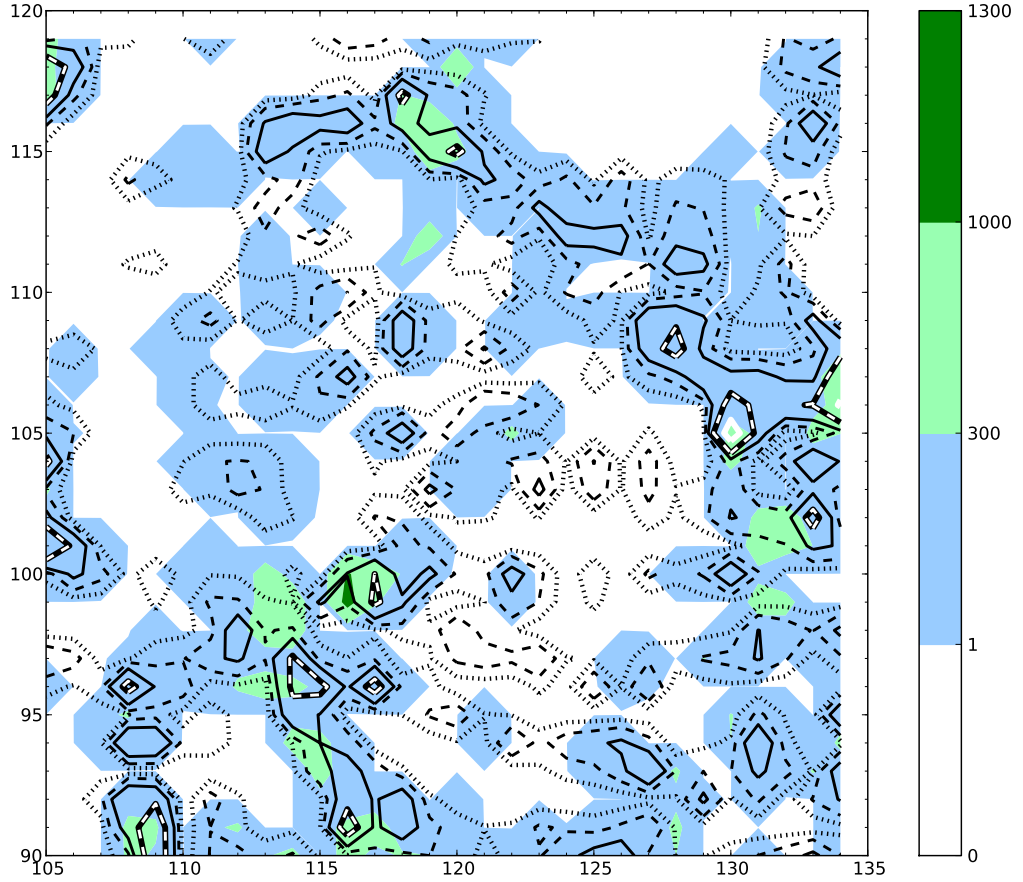


**Figure 7.** A zoomed low density region in the top right corner of Fig. 5 and 6. The filled contours show the values of  $\sigma_v^2$  as indicated by the color column. The black and white contour lines show a few density peaks above unity in units of the mean density. The solid, dashed and dotted lines correspond to  $\rho = 0.5, 0.25$  and  $0.1$  respectively. The heavy white line at about  $(130, 105)$  shows one small contour with  $\rho = 2$ .

### 6.1 The slice through a void

The region from the top right corner of the slice is zoomed in Fig. 7. The color map is changed again in order to adopt better for the low density environment. The levels of  $\sigma_v^2$  are shown by the color column while the density contours are shown by black lines. The density in the most of the region is below the mean except a few peaks shown by black and white heavy line. The impression is similar to that from Fig. 5: the fields have many similarities but also substantial differences, perhaps even a little greater differences than in Fig. 5. In particular, the empty regions seem to be significantly more empty in  $\sigma_v^2$  than in  $\rho$  in an agreement with the discussion in Sec. 5. Although the density contours are pushed to such a low values that one may completely disregard them as being subgrid noise the values of the  $\sigma_v^2$  contours are also very low and still there is some similarity between both fields in some



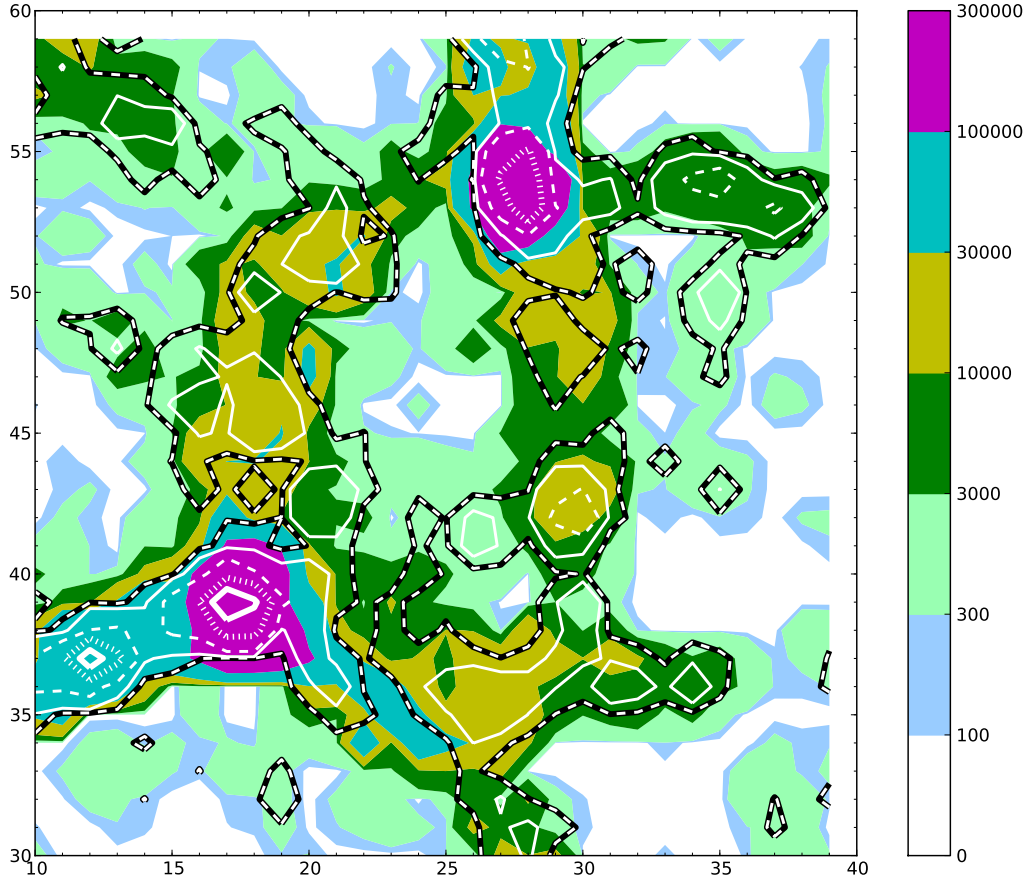


**Figure 8.** A zoomed high density region in the bottom left corner of Fig. 5 and 6. Here, filled contours correspond to  $\sigma_v^2$  as indicated by the color. The black and white line shows contours of  $\rho = 1$ , and white solid, dashed, dotted and heavy solid contours correspond to  $\rho = 3, 10, 30$ , and  $60$  respectively.

parts of the figure. Thus, an optimistic conclusion would be that the combination of both fields may allow to probe low density regions more reliably than any of them alone. On the other hand, a pessimistic conclusion would relate it to the correlation of the  $\rho$  and  $\sigma_v^2$  fields at small  $\sigma_v^2$ . The further study is obviously required.

## 6.2 The slice through clumps and filaments

Figure 8 shows the relatively high density region in the bottom left corner of Fig. 5 and 6. The figure contains a few density peaks with  $\rho > 10$  (white dashed lines) three of which are higher than  $\rho = 30$  and two even higher with  $\rho > 60$ . There are also a few filaments connecting the clumps. Again the both fields are rather similar but there are notable differences as well. Two highest density peaks in the bottom left corner reach  $\rho > 60$  but only one exceeds  $\sigma_v^2 > 10^5$ . However, the peak of  $\sigma_v^2$  extends to the density level as low as the mean density.

On the other hand a little lower density peak with  $\rho < 60$  coincides with a quite substantial region with  $\sigma_v^2 > 10^5$ . Similar observations can be made with the peaks of lower density. Thus, we conclude that the density and  $\sigma_v^2$  are two parameters that have a substantial degree of independence and therefore may better characterize the clumps and filaments as any of them alone. In addition, the figure shows that the filaments are the multi-stream flows in agreement with both the TZA and AA models and contrary to the prediction of the BKP model that implies that the filaments have not reached the state of multi-stream flows.

## 7 The mean velocity field

Finally, we present the mean velocity field defined by eq. 2.3. We superimpose the mean velocity field shown by the arrows on Fig. 8 where we keep only three highest levels of the density contours for clarity.

The highest density peak sitting at the largest patch of high  $\sigma_v^2$  is in the bottom left corner approximately at (17, 39). The overall pattern of the mean velocity field clearly indicates that the whole region shown in the figure is falling on this clump. The mass inside three filaments is streaming toward the clump confirming one of the predictions of the AA model [15]. The second largest clump at (28, 54) is falling on the first clump accompanied by the surrounding filaments. The filaments are highly inhomogeneous and the streams are far from being uniform. The velocity field in the vicinity of the first clump looks roughly circular giving the impression of quasi-spherical (actually quasi-circular in this plane because we see only the cross section) accretion but this is misleading if we look at the flux of mass  $\rho \bar{\mathbf{v}}$  shown by arrows in Fig. 10. It is worth stressing that in order to accommodate the arrow lengths in the figure, their lengths are made proportional to the square root of the magnitude instead of the magnitude. Thus the difference between the fluxes from three adjacent filaments compared to that from three surrounding voids is considerably more dramatic than it appears in the figure.

## 8 Summary

We present a new numerical technique that allows to identify the multi-stream flows, *i.e.* the regions where the velocity field is multi-valued. According to [32] these regions have reached a clear physical threshold to be identified as being in strong nonlinear regime but most of them are not virialized. The multi-stream flows form the web overall very similar by appearance to the web identified in the density field. At the same time many features are very different both in low and high density environments as seen in Fig. 7 and 8. These include the difference of the shapes of the contours around peaks, the lack of monotonic relation between the heights of peaks in the  $\rho$  and  $\sigma_v^2$  fields. Although one can see a positive correlation between the density and the  $\sigma_v^2$  that determines the multi-stream flows in Fig. 3, the spread of points along both axes ( $\rho$  and  $\sigma_v^2$ ) is very large suggesting that these parameters are quite independent. Therefore  $\sigma_v^2$  may serve as a second parameter characterizing the dynamical environment in the nonlinear density peaks before they reached virial equilibrium as well as for filaments and pancakes. The method for computing  $\sigma_v^2$  is localized in Eulerian coordinates and is very easy to implement.

Ideally  $\sigma_v^2$  is identically equal to zero everywhere where the velocity is singled-valued but the simplest numerical implementation based on the ordinary CIC method generates noise. Although it is seemingly not posing a serious problem other schemes like TSC (triangular



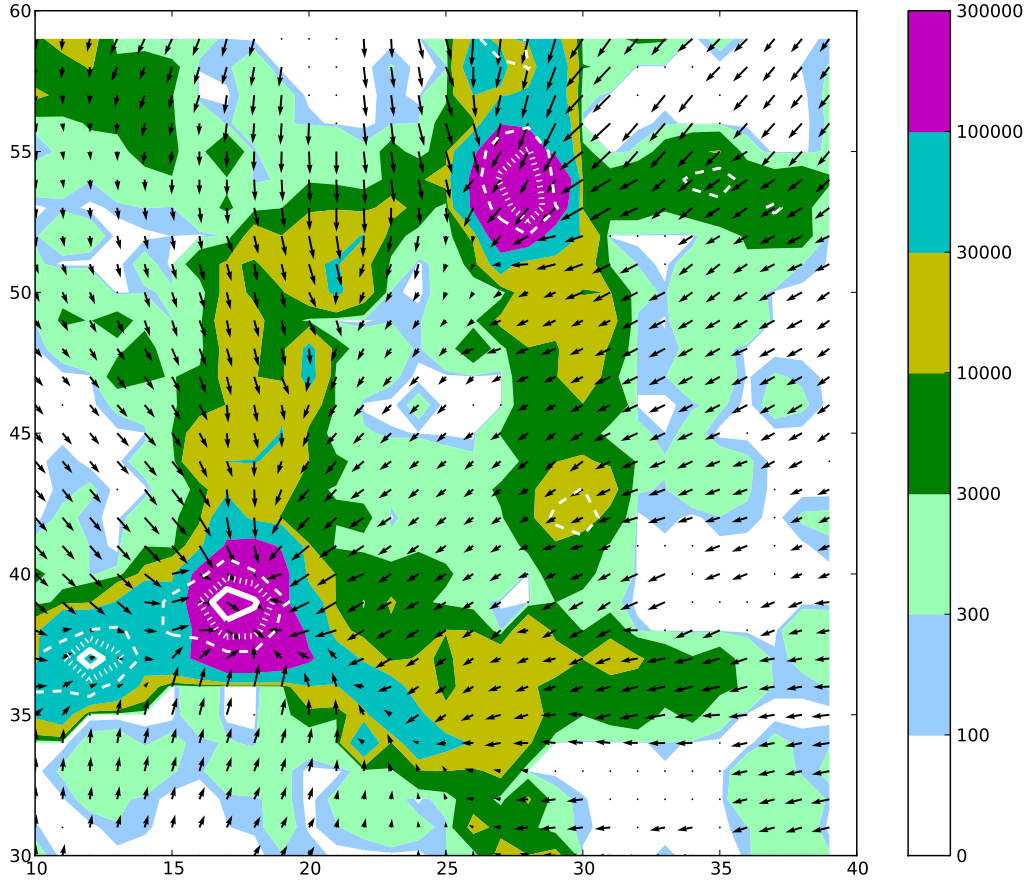


**Figure 9.** The mean velocity field  $\bar{v}$  projected on the slice plane is superimposed on the  $\sigma_v^2$  field shown in Fig. 8. White contours show peaks with density above 10, 30 and 60 in the units of the mean density with dashed, dotted and heavy solid lines respectively.

shape density cloud) may be less noisy. This will be checked and reported in the following publications.

The field  $\sigma_v^2$  naturally defines the physical condition for voids as the regions devoid of multi-stream flows. The identification of the multi-stream flows of course depends on the resolution (in particular the mass resolution) of the simulation, but this is the fundamental limitation for all fields obtained in the simulations. The  $\sigma_v^2$  field by no means is worse than commonly used density field in this respect. This condition is physically more clear than one based on an essentially arbitrary density threshold. It is worth stressing that about 22% of the total volume has nonzero density but no multi-stream flows. For the resolution of the  $\Lambda$ CDM simulation used here ( $\approx 1 h^{-1}\text{Mpc}$ ) we find the volume fraction in voids is at least about one third of the total volume. This is considerably greater than at the percolation transition evaluated for a similar simulation in [28], therefore the volume devoid of multi-stream flows consists predominantly of one connected region.

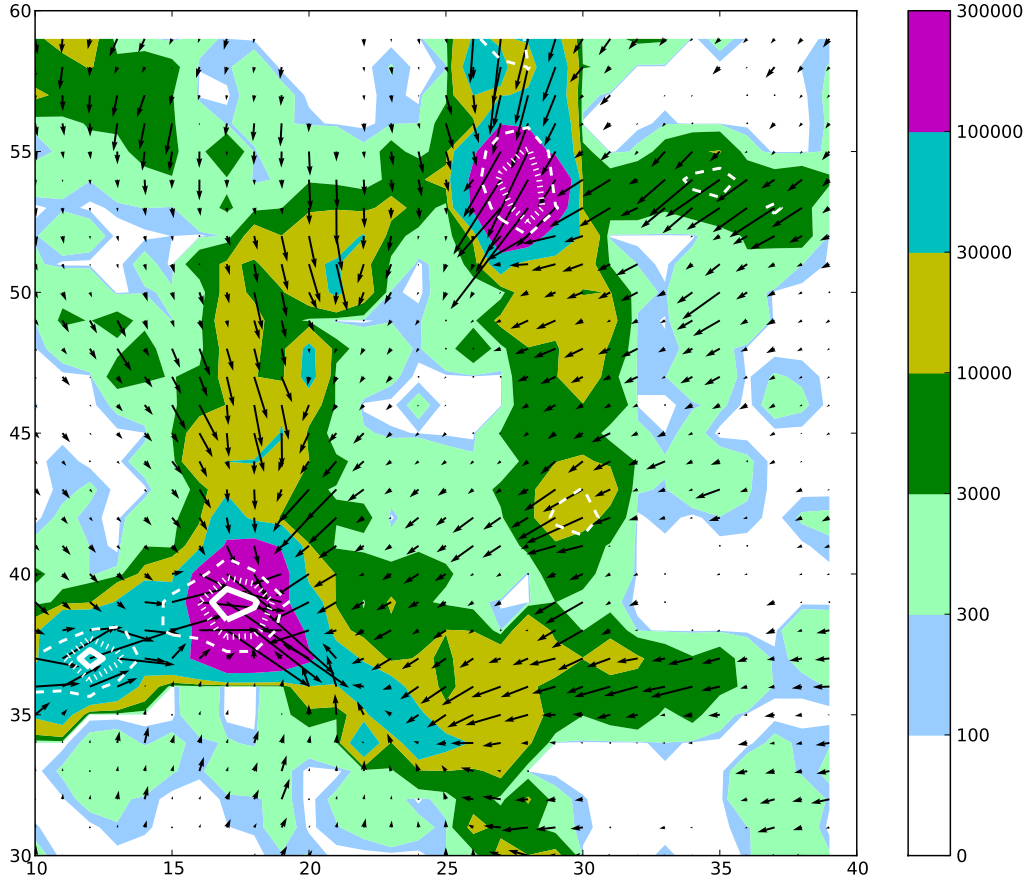


**Figure 10.** The flux of mass  $\rho\bar{\mathbf{v}}$  is shown by arrows. The color scheme and contours are the same as in Fig. 9. In order to accommodate the length of arrows their lengths are made proportional to the square root of the magnitude.

The mean velocity field  $\bar{v}_i$  defined by eq. 2.3 shows the mass flow along the filaments toward the clumps in agreement with the prediction of the adhesion approximation [15]. Some filaments seem to move predominantly in the transverse direction as a whole (see Fig. 9). The mean velocity field seems to be quite smooth without significance convergence in these cases. A somewhat similar observation can be made concerning the clumps. In some of them as in one at (17, 39) in Fig. 9 and 10 the velocity field seems to converge significantly stronger than in the other similar clump at (28, 54) in the same figures where the velocity field looks significantly more steady.

The filaments with lengths over  $50 h^{-1}$  are shown to be the multi-stream flows in a qualitative agreement with both the truncated Zeldovich approximation [9] and the adhesion approximation [15].

Summarizing, we would like to stress the importance of the study of dynamics in filaments and pancakes, which are highly nonlinear but unvirialized dynamical systems. The

suggested technique may be a useful tool to serve this purpose.

**Acknowledgments** The author is grateful to Salman Habib and Katrin Heitmann for providing the results of N-body simulation.

## References

- [1] Aragón-Calvo M A, Jones B J T, van de Weygaert R, van der Hulst J M, *The multiscale morphology filter: identifying and extracting spatial patterns in the galaxy distribution*, 2007 Astron. Astrophys. **474** 315
- [2] Aragón-Calvo M A, Platen E, van de Weygaert R, Szalay A S, *The spine of the cosmic web*, 2010 Astrophys. J. **723** 364
- [3] Arnold V I, Shandarin S F, Zel'dovich Ya B, *The large-scale structure of the universe I. general properties. One- and two-dimensional models* 1982 Geophys. Astrophys. Fluid Dynamics **20** 111
- [4] Bardeen J, Bond J R, Kaiser N, Szalay A S, *The statistics of peaks of Gaussian random fields*, 1986 Astrophys. J. **304** 15
- [5] Bond J R, Kofman L, Pogosyan D, *How filaments of galaxies are woven into the cosmic web*, 1996 Nature **380** 603
- [6] Bond N A, Strauss M A, Cen R, *Crawling the cosmic network: exploring the morphology of structure in the galaxy distribution*, 2010 Mon. Not. Roy. Astron. Soc. **406** 1365
- [7] Bond N A, Strauss M A, Cen R, *Crawling the cosmic network: identifying and quantifying filamentary structure*, 2010 Mon. Not. Roy. Astron. Soc. [arXiv:1003.3237]
- [8] Buchert T, *Lighting up pancakes - Towards a theory of galaxy formation*, 1989 Rev. Mod. Astr. **2** 267
- [9] Coles P, Melott A, Shandarin S F, *Testing approximations for non-linear gravitational clustering*, 1993 Mon. Not. Roy. Astron. Soc. **260** 765
- [10] Doroshkevich A G, Shandarin S F, *A statistical approach to the theory of galaxy formation*, 1978 Sov. Astron. **22** 653
- [11] Doroshkevich A G, Shandarin S F, *A mean density and a correlation function of rich clusters: theory and observations*, 1978 Mon. Not. Roy. Astron. Soc. **182** 27
- [12] Doroshkevich A G, Kotok E V, Novikov I D, Polyudov A N, Shandarin S F, Sigov Yu S, *Two-dimensional simulation of the gravitational system dynamics and formation of the large-scale structure of the universe*, 1980 Mon. Not. Roy. Astron. Soc. **192** 321
- [13] Fillmore J A, Goldreich P, *Self-similar gravitational collapse in an expanding universe*, 1984 Astrophys. J. **281** 1
- [14] Forero-Romero J E, Hoffman Y, Gottlöber S, Klypin A, Yepes G, *A dynamical classification of the cosmic web*, 2009 Mon. Not. Roy. Astron. Soc. **396** 1815
- [15] Gurbatov S N, Saichev A I, Shandarin S F, *The large-scale structure of the universe in the frame of the model equation of non-linear diffusion*, 1989 Mon. Not. Roy. Astron. Soc. **236** 385
- [16] Habib S, et al. *Hybrid petacomputing Meets Cosmology: The Roadrunner Universe Project*, 2009 Journal of Physics: Conference Series **180** 012019
- [17] Hahn O, Porciani C, Carollo C M, Dekel A, *Properties of dark matter halos in clusters, filaments, sheets and voids*, 2007 Mon. Not. Roy. Astron. Soc. **375** 489
- [18] Klypin A A, Shandarin S F, *Three-dimensional numerical model of the formation of large-scale structure in the universe*, 1983 Mon. Not. Roy. Astron. Soc. **204** 891

- [19] Kofman L, Pogosyan D, Shandarin S F, Melott A L, *Coherent structures in the universe and the adhesion model*, 1992 *Astrophys. J.* **393** 437
- [20] Little B, Weinberg D, Park C, *Primordial fluctuations and non-linear structure*, 1991 *Mon. Not. Roy. Astron. Soc.* **253** 295
- [21] Maciejewski M, Vogelsberger M, White S D M, Springel V, *Bound and unbound substructures in Galaxy-scale Dark Matter haloes*, 2010, arXiv:1010.2491
- [22] Melott A L, Shandarin S F, *Gravitational instability with high resolution*, 1989 *Astrophys. J.* **343** 26
- [23] Melott A L, Shandarin S F, Weinberg D, *A test of the adhesion approximation for gravitational clustering*, 1994 *Astrophys. J.* **428** 28
- [24] Novikov D, Colombi S, Doré O., *Skeleton as a probe of the cosmic web: the two-dimensional case*, 2006 *Mon. Not. Roy. Astron. Soc.* **366** 1201
- [25] Peebles P J E , *Large Scale Structure of the Universe*, 1970 , Princeton Univ. Press
- [26] Platen E, van de Weygaert R, Jones B J T., *A cosmic watershed: the WVF void detection technique*, 2007 *Mon. Not. Roy. Astron. Soc.* **380** 551
- [27] Pope A, Habib S, Lukic Z, Daniel D, Fasel P, Desai N, Heitmann K, *The accelerated Universe*, 2010 *Computing in Science and Engineering* **12** 17
- [28] Shandarin S F, Sheth J, Sahni V, *Morphology of the supercluster-void network in  $\Lambda$ CDM cosmology*, 2004 *Mon. Not. Roy. Astron. Soc.* **353** 162
- [29] Shandarin S F, Zeldovich Ya B, *The large-scale structure of the universe: Turbulence, intermittency, structures in a self-gravitating medium*, 1989 *Rev. Mod. Phys.* **61** 185
- [30] Weinberg D H, Gunn J, *Simulation of deep redshift surveys*, 1990 *Astrophys. J.* **325** L25
- [31] Weinberg D H, Gunn J, *Large-scale structure and the adhesion approximation*, 1990 *Mon. Not. Roy. Astron. Soc.* **247** 260
- [32] Zeldovich Ya B, *Gravitational instability: An approximate theory for large density perturbations*, 1970 *Astron. Astrophys.* **5** 84